Journal of Applied Fluid Mechanics, Vol. 12, No. 4, pp. 1189-1202, 2019.
Available online at www.jafmonline.net, ISSN 1735-3572, EISSN 1735-3645.
DOI: 10.29252/jafm.12.04.29579

CFD Study of the Effect of Geometrical Shape of Separation Blades on the Rotor Performance of an Annular Centrifugal Extractor (ACE)

H. Ghaya[1†], R. Guizani[1], H. Mhiri[1] and P. Bournot[2]

[1] *University of Monastir, National Engineering School of Monastir (ENIM), UTTPI, Av. Ibn El Jazzar, 5019 Monastir, Tunisia*
[2] *IUSTI, Technopôle de Château-Gombert, 5 rue Enrico Fermi, 13 013 Marseille, France*

†*Corresponding Author Email: hanane_ghaya@yahoo.fr*

(Received August 27, 2018; accepted November 23, 2018)

ABSTRACT

Annular centrifugal extractors have a great potential in the multiphase extraction of pharmaceutical, nuclear, and many other processes. Although the widespread use of this device, the design procedures are still unavailable because of the complexity of the fluid mechanics in the rotor region called the separation zone. From a structural point of view, this region has a complicated conception due to the different internals. This study presents a three-dimensional numerical simulation of the flow field inside the rotor region of an annular centrifugal extractor ACE. The industrial CFD code (Fluent) was used to model the highly swirling fluid flow in the settling zone with various geometries of separation blades (straight blades and curved blades). Numerical predictions and experimental results were compared in order to validate the proposed models. The velocity field with the k-ε model shows a good agreement with the experimental data available in the literature. The Volume of Fluid (VOF) method was employed to simulate the physics of the interface of air/water free surface. A comparison between the flow field and the performances of the ACE model design with vertical straight blades and with vertical curved blades was further investigated to study the effect of the geometric shape of the separation blades on the parameters of liquid holdup volume, the interface radius and the pressure drop. It was found that the geometry of the separating blades has a significant impact on the pressure drop, liquid hold-up volume and interface radius and general flow in the extractor-settling zone. The predicted pressure drop proved that the geometry of the ACE rotor with curved blades leads to a lower values of pressure drop.

Keywords*:* CFD; ACE rotor ; Multi-phase flow; Pressure drop; The interface radius; Liquid holdup volume.

NOMENCLATURE

a	diameter of the light phase outlet
CFD	Computational Fluid Dynamics;
D	diameter of the rotor
g	gravitational acceleration
hd	distance between the inlet and the diverter disc
k	turbulent Kinetic energy
MRF	Multiple Reference Frame
P	pressure
rpm	revolution per minute
r	radial distance
r_i	interface radius
R	radius of the rotor
Rd	radius of the diverter disc
Re	Reynolds number, dimensionless
t	time
$\overrightarrow{U_r}$	Whirl velocity (velocity due to the moving frame)
$\overrightarrow{V_r}$	Relative velocity
$\vec{V}$	absolute velocity
w	angular velocity(rad/s)
ε	turbulent energy dissipation rate
ρ	density
μ	molecular viscosity
ν	kinematic viscosity
ω	angular velocity
α_i	volume fraction

Subscripts

i, j, k	indices in coordinate direction;

1. INTRODUCTION

The multiphase extraction technique or solvent extraction is used to separate one or more components from a homogeneous fluid mixture. A very attractive device to integrate chemical reaction and separation for multiphase systems is the annular centrifugal contactor ACC or extractor ACE. The ACE has been developed at the Argonne National Laboratory in the USA in 1960s. An improved version was patented by Costner Industries Nevada Corporation. This device mainly include a rotating hollow centrifuge that was been called a rotor in a stationary house (Boelo Schuur, N. Kraai, G.M.Winkelman, & J. Heeres, 2012). The two immiscible process fluids enter the equipment in the annular zone between the fixed wall and the moving rotor, where they are intensely mixed. Afterwards, they are transported into the centrifuge through a hole in the bottom where separation occurs by the action of centrifugal forces.

Annular centrifugal extractors are widely used in several industrial fields for the extraction of radioactive fuel in nuclear fuel reprocessing where safety is the concern (Bernstein, Grosvenor, Lenc, & Levitz, 1973), in biological operations, in agro-food applications, in chemical and pharmaceutical industries such as the synthesis of powdered silica particles and the regeneration of spent activated carbon. This equipment can also be used in metal recycling, in emulsion polymerization (Imamura, Saito, & Ishikura, 1993) (Kataoka, Ohmura, Kouzu, Simamura, & M.Okubo, 1995), in hydrometallurgical processes (Jing, Ning, Cao, Wang, & & Sun, 2018) (Zhou, Duan, Zhou, & Zhang, 2007), in wastewater treatment and in many other processes. Annular centrifugal extractors could also be used for a variety of chemical reactions such as synthesis of monodisperse silica particles (Ogihara, et al., 1995), esterification and hydrolysis (Gandhi, Sawant, & Joshi, 1995).

The annular centrifugal extractors provide several advantages in the multiphase extraction process over other conventional process. The equipment provides a very high centrifugally accelerated settling, excellent separation of phases and quick start-up time than conventional extractors such as pulse columns or mixer settlers, small hold up volume, low residence time, high throughput and very high mass transfer efficiency.

Because of the above advantages, much experimental work on annular centrifugal extractors has been performed through the 1980s by ANL researchers. The effort was first focused on analytical approaches and descriptive correlation of experimental data. An analytical methods and experimental correlations based on hydrostatic balance arguments have been developed to determine the proper dimensions of ACE weirs (Leonard, Bernstein, Pelto, & Ziegler, 1981) (Leonard, Ziegler, & Bernstein, 1980) Most of the design optimization of annular extractors was based on operating experiences like Arafat *et al.* (Arafat, Hash, Hebben, & Leonards, 2001). In fact, the estimation of proper settling zone height is very critical in the design of a separator zone.

Despite the experimental and the analytical researches that have been carried out on the ACE, the major part of the reported design predictions and analysis of the results has been mostly through flow sheet simulations, which treat the operation as a black box. Computational fluid dynamics (CFD) provides a useful tool for solving the above problems. However, there is a lack of literature focusing on the separation region of the ACE; several reports have been published on CFD studies of the centrifugal extractor order to reduce empiricism. Most of the authors have investigated the fluid mechanics of single and multiphase flow in the annular zone (Wardle K. , Allen, Anderson, & Swaney, 2009) (Wardle K. E., Allen, Anderson, & Swaney, 2008) (Deshmukh, Vedantam, Joshi, & Koganti, Computational flow modeling and visualization in the annular region of annular centrifugal extractor, 2007) (Deshmukh, Vedantam, & Joshi, Flow Visualization and Three-Dimensional CFD Simulation of the Annular, 2008) (Sathe, Deshmukh, Joshi, & Koganti, 2010) (Shaowei, Wuhua, Jing, & Jianchen, 2012). For instance, Collins *et al.* (Padial-Collins, Zhang, Zou, & Ma, 2006) have simulated the separation of an aqueous and organic stream in the rotor zone. This simulation did not consider the flow of the air-Liquid interface within the rotor.

As the experimental studies are often limited by their high cost related to the measurement techniques (Chouari, Kriaa, Mhiri, & Bournot, 2017), (Yan, Jian-gang, Shuang-liang, & Zhi-shan, 2015) have experimentally examined the flow field by changing only the speed of rotation and the flow rate. To overcome these limits and provide a general way to estimate the multiphase extraction process phenomena, we propose, in this study, a detailed numerical investigation on the effect of several operating parameters (rotation speed of rotor, etc.) for a variety range of values and different designs of the rotor on the performance of the ACE.

In the present work, CFD simulations of the flow pattern of an Annular Centrifugal Extractor rotor was investigated. This study aims to validate the experimental results made by Xu *et al.* (Yan, Jian-gang, Shuang-liang, & Zhi-shan, 2015). We tried also to study the three dimensional, complicated, high swirling flow pattern inside the rotating rotor. This work also aims to compare by simulation the flow field in the rotor of different designs with straight internals and curved internals. It is to be noted that the performance improvement of the ACE requires a complex structure and additional operating costs. Therefore, a better understanding of the flow field is needed to make further design improvements (Achouri, Mokni, Mhiri, & Bournot, 2012).This study provide a more complete understanding of the flow inside the moving rotor in order to gain the confidence to go further and model increasingly more complex cases.

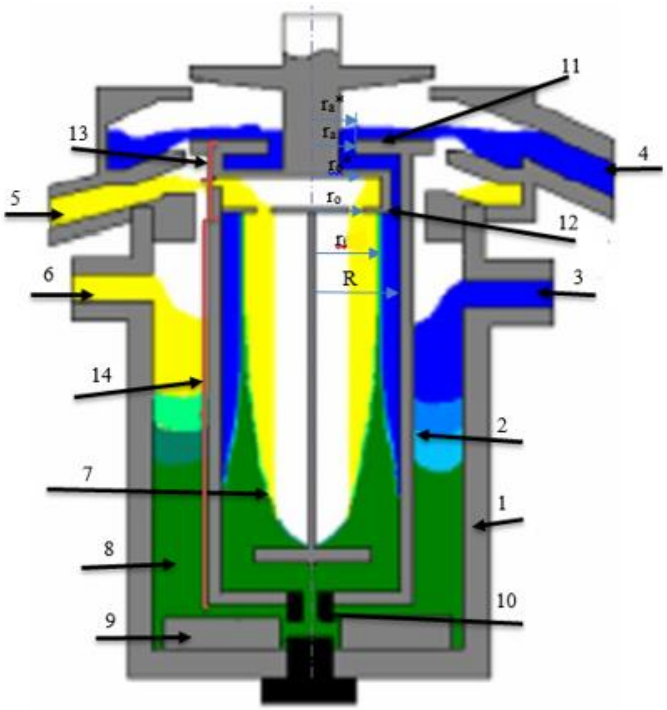

1-Housing	*6-light phase inlet*	*11-heavy phase weir*
2-Rotor	*7-Separating blades*	*12-light phase weir*
3-heavy phase inlet	*8-Annular mixing zone*	*13-weirs section*
4-heavy phase outlet	*9-Radial vanes*	*14-separating zone*
5-light phase outlet	*10-Rotor inlet*	

Fig. 1.General view of the annular centrifugal extractor (ACE).

2. OPERATING PRINCIPALS

The design of two concentric cylinders where the Inner cylinder rotates and the outer stationary one is based on the Taylor- Couette principle. The equipment is schematically shown in Fig. 1. The flows of the immiscible fluids enter through the tangential ports light phase inlet and heavy phase inlet into the region of the annular mixture. Indeed, it forms the form of dispersion while the fluids mix by the shear induced by the rotation of the rotor. The rotor region can include different equipment that is used to improve the separation process such as the radial vanes. The centrifuge separates the two phases and pumps the fluids upwards. The separate phases, then, flow by gravitation to their respective weirs and out of the outlet lines. Thus, the annular centrifugal extractor acts as a mixer, centrifuge and pump. From a structural point of view, the annular centrifugal extractor can be divided into two zones: the mixing zone and the separation zone. The mixing zone is located in the annular zone in which the two-phase mass transfer process is mainly controlled by the flow field. The field of flow in

this zone is studied in depth by numerical simulation and experimental methods. The separation zone was composed of the rotor and the weir zones. This region is much more complicated due to the presence of the different internals. The flow field in the rotor region directly affects the efficiency of the annular centrifugal extractor. Therefore, a better understanding of the flow field is needed to make further design enhancements.

3. COMPUTATIONAL FLUID DYNAMICS

To estimate the flow pattern and the pressure field precisely, unsteady CFD simulations were performed. In our case, three-dimensional simulations have been carried out for the multiphase system.

3.1 Computational Geometry and Grid

The considered geometry is the separating zone of an annular centrifugal extractor (ACE) with two different shapes of vertical separating blades (four straight blades and four curved blades). The studied geometries consisted of the rotor and the weir zones. This region is much more complicated because of the presence of the various internals such as the diverter disc as well as the separation blades (the vertical fins). As this geometry is quite complex, the most important dimensions of the 50 mm model rotor geometry are taken from the experimental study of Xu *et al.* (Yan, Jian-gang, Shuang-liang, & Zhi-shan, 2015). Figure 2 and Fig. 3 Show a general view of the studied separating region of the ACE and its dimensions notations.

The mesh generated of the ACE rotor is hybrid. We

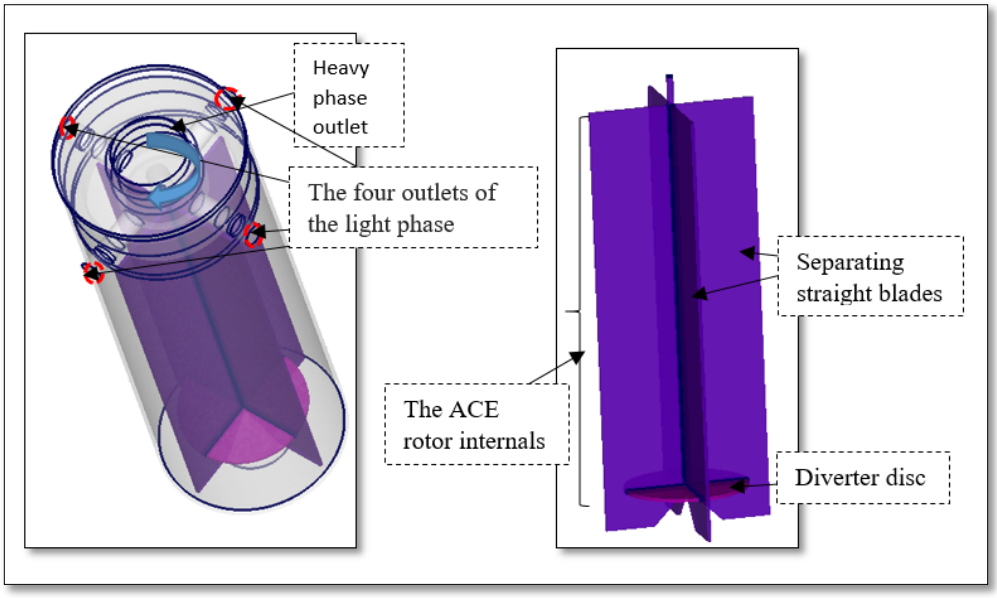

Fig. 2. General view of the studied separating region of the ACE rotor.

tried to generate a maximum of hexahedral cells with refinement in the critical zones like the central region and near the walls. The computational domains consist of 583, 098 and 711, 017 CFD cells for ACE rotor with straight blades and rotor with curvedblades respectively. This work was simulated using the "Fluent" software. Grid independency tests have been studied for both types of the ACE rotors and the chosen meshes were the best ones. In fact, for each type of the ACE rotor, we tested three numbers of grids, and we found out that the chosen mesh and the finer mesh gave the same values of velocity distribution profiles and pressure drop, which led us to the choice of the presented meshes.

The strength of the numerical results is highly depending on the modeling of the flow in the region near the walls of the ACE rotor. **y+** is a non-dimensional distance from the wall. It describes the fineness of the mesh in the wall-bounded flows. The y+ used in this study was 30. While the non-equilibrium wall functions are employed to solve the solution near the wall region. In the inlet, we have a mixture of air and water with the same volume fraction of 0.5.The inlet boundary condition was defined by velocity inlet equal to 0.1 m /s, and the outlet was defined by pressure outlet. All the walls had no-slip boundary conditions. The surface tension was included with the value of 72 dynes /cm (air/water interfacial tension) the water contact angle on all surfaces was set at 75° (Wardle, Allen, & Swaney, CFD simulation of the separation zone of an annular centrifugal contactor, 2009). The ambient pressure was fixed to be atmospheric pressure. Figure 4 is an overall view of the generated grid and zooms in the four integrated vertical blades and the light phase outlets of the fluid for the different studied designs of the ACE rotors.

3.2 Numerical Scheme

The used multiphase model is the so-called VOF free surface multiphase flow model, which is the best model to simulate the interface between the liquid and the air in the separating zone of annular centrifugal extractor and describe the hydrodynamics of the flow.

This model simulates two or more fluids (or phases) which are not interpenatring and it is used to simulate bubble motion and to track the free surface flows. .

In order to reduce computational costs and keeping the same accuracy the multiple reference frames (MRFs) model was employed to simulate the rotational extractor.

The Reynolds numbers (*Re*) (Patra, Pandey, Muduli, Natarajan, & Joshi, 2013) is given by: $Re = \frac{w.R.\rho.D}{\mu}$

In the present work, we have varied the angular velocity from 590 rpm to 4000 rpm. The range of *Re* found 76819 to 520776. A high Reynolds number indicates a high inertia and consequently a turbulent flow. Therefore, in the actual rotor; the flow can be considered as turbulent.

In this numerical study, turbulence was modeled using the standard k–ε model. This model is essentially a high Reynolds number model and assumes that the flow is fully turbulent and the effects of molecular viscosity are negligible.

We will discuss the details of the flow governing equations further in this work.

3.3 Governing Equations

We consider a two-phase flow implying an incompressible liquid and a compressible gas in the turbulent regime. The surface tension effects are taken into account. The tested fluids are air and water, which have been assumed Newtonian and immiscible. The flow is unsteady and isothermal.

Given the above assumptions, the governing equations (Khaldi, Mhiri, & Bournot, 2014) can be written as follows:

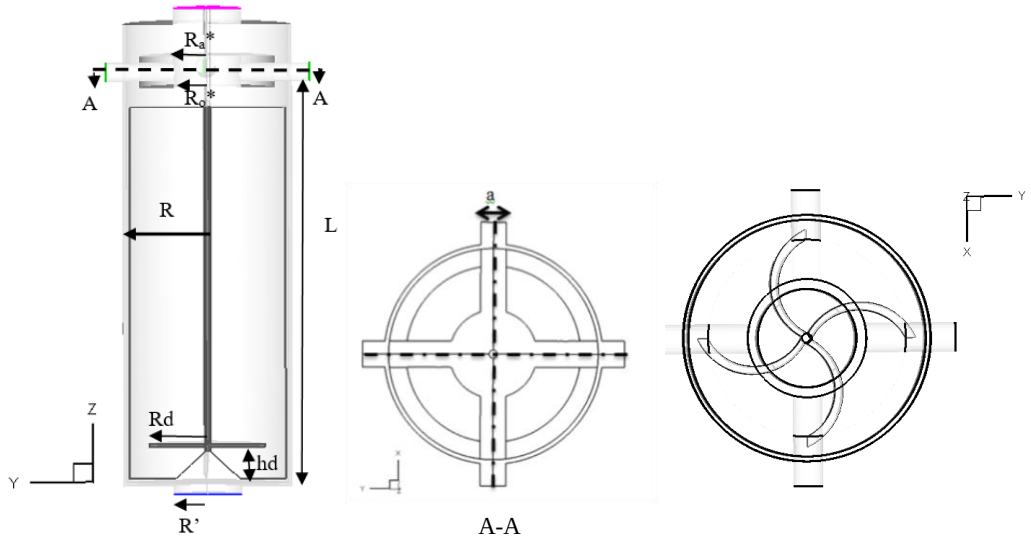

(a) The basic geometry of the ACE rotor

(b) The proposed modification of curved blades

R	R'	R*o	Ra*	Rd	hd	L	a	*All dimensions are in mm*
25	10	10	12	17	10	120	10	

Fig. 3. Geometries and Dimensions of the studied domains (Yan, Jian-gang, Shuang-liang, & Zhi-shan, 2015).

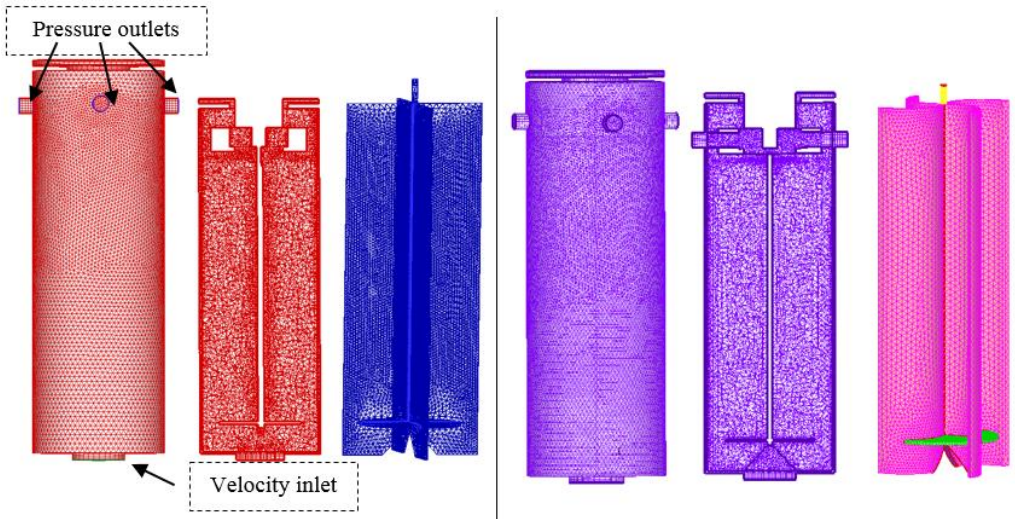

Fig. 4. CFD grid of the studied domain and boundary conditions.

Continuity

$$\frac{\partial \rho}{\partial t}+\frac{\partial(\rho u_i)}{\partial x_i}=0 \tag{1}$$

Momentum

$$\rho\frac{\partial(\rho u_i)}{\partial t}+u_i\frac{\partial(\rho u_i)}{\partial x_i}=\frac{\partial(\tau_{ij})}{\partial x_j}+\frac{\partial p}{\partial x_i}+\rho g_i+S_{i,s} \tag{2}$$

Where, ρ is the density, u_i is the three velocity components, p is the pressure, and τ_{ij} is the Reynolds stress tensor.

3.3.1 VOF Model

To model the sharp fluid–fluid interfaces using a finite volume approach, the VOF method is very suitable. It has been verified that it is appropriate for acquiring and tracking a free surface (Mokni, Dhaouadi, Bournot, & Mhiri, 2015) (Achouri, Mokni, Mhiri, & Bournot, 2012) (Padial-Collins, Zhang, Zou, & Ma, 2006) (Wardle K. E., Allen, Anderson, & Swaney, 2008) (Wardle, Allen, &

Swaney, CFD simulation of the separation zone of an annular centrifugal contactor, 2009).

The tracking of the interface between the two phases is done by a color function (phase indicator function) that shows the fractional amount of fluid at a some position. The interface tracking between the two phases is done with the solution of the continuity equation (Eq. 1) for the secondary phase (air is set as the secondary phase in this study,). Then, the interface is reconstructed using the geometric reconstruction (Geo-reconstruct) method. This method can simulate efficiently flows including the shape and evolution of the free surface (Khaldi, Mhiri, & Bournot, 2014). That is why this model can simulate flows including the shape and evolution of the free surface in the separating zone of the annular centrifugal extractor.

This interface is calculated with the following equation:

$$\frac{\partial(\alpha_2\,\rho_2)}{\partial t}+\frac{\partial(\alpha_2\,\rho_2 U_i)}{\partial x_i}=S_2 \tag{3}$$

Where S_2 is the source of the phase 2 (in this study S_2 is equal to zero), ρ_2 is the density of the secondary phase and α_2 is the volume fraction of the secondary phase (α_2 =V2/V).V is the total volume of fluids (V=V_1+V_2), V_1 is the volume of phase 1 and V_2 is the volume of phase 2.

The volume fraction of the primary phase (α_1=V_2/V) is deduced by the constrain:

$$\sum_{i=1}^{2}\alpha_i=1 \tag{4}$$

In the momentum Eq. (2), the interaction between the phases is modeled by the surface tension $S_{i,s}$.

3.3.2 Standard k-ε Model

The standard k-ε model of turbulence is a semi empirical model constructed on model transport equations for the turbulence kinetic energy (k) and its dissipation rate (ε). It is based on the Boussinesq hypothesis, which assumes that the Reynolds stress is proportional to the mean velocity gradient, with the constant of proportionality being the turbulent viscosity. This quantity is assumed by the following equations:

$$\nu_t=C_\mu\frac{k^2}{\varepsilon} \tag{5}$$

Where $C_\mu$is an empirical constant of the standard k–ε model.

The model transport equation for k is derived from the exact equation, while the model transport equation for ε was obtained using physical reasoning and bears little resemblance to its mathematically exact counterpart.

The turbulence kinetic energy, k, and its rate of dissipation, ε, are obtained from the following transport equations (FLUENT 6.3, 2001):

k equation:

$$\frac{\partial(\rho k)}{\partial t}+\frac{\partial\left(\rho k\overline{U_i}\right)}{\partial x_i}=\frac{\partial}{\partial x_j}\left[\left(\mu+\frac{\mu_t}{\sigma_k}\right)\frac{\partial k}{\partial x_j}\right]+G_k+G_b-\left(\rho\varepsilon+Y_M\right) \tag{6}$$

ε equation:

$$\frac{\partial(\rho\varepsilon)}{\partial t}+\frac{\partial\left(\rho\varepsilon\overline{U_i}\right)}{\partial x_i}=\frac{\partial}{\partial x_j}\left[\left(\mu+\frac{\mu_t}{\sigma_\varepsilon}\right)\frac{\partial\varepsilon}{\partial x_j}\right]+C_{1\varepsilon}\frac{\varepsilon}{k}\left(G_k+C_{3\varepsilon}G_b\right)-C_{2\varepsilon}\rho\frac{\varepsilon^2}{k} \tag{7}$$

In these equations, G_k represents the generation of turbulence kinetic energy due to the mean velocity gradients. G_b is the generation of turbulence kinetic energy due to buoyancy. Y_M represents the contribution of the fluctuating dilatation in compressible turbulence to the overall dissipation rate. $C_{1\varepsilon}$,$C_{2\varepsilon}$, and $C_{3\varepsilon}$ are constants. σ_k and $\sigma_\varepsilon$are the turbulent Prandtl numbers for k and ε, respectively.

3.3.3 MRF Model

The Multiple Reference Frame model is a steady state approach, which can provide a reasonable model for many applications such as the rotational flow in the ACE equipment. The computational domain for the numerical problem is defined with respect to the rotating frame such that an arbitrary point in the computational domain is located by a position vector $\vec{r}$ from the origin of the rotating frame.

The following relation is used to transform the fluid velocities from the stationary frame to the rotating frame (FLUENT 6.3, 2001):

$$\overrightarrow{V_r}=\vec{V}-\overrightarrow{U_r} \tag{8}$$

Where

$$\overrightarrow{U_r}=\vec{\omega}*\vec{r} \tag{9}$$

Where $\overrightarrow{V_r}$ is the relative velocity,

$\vec{V}$ is the absolute velocity,

$\overrightarrow{U_r}$ is the "whirl" velocity (the velocity due to the moving frame).

Solving the equations of motion in the rotating frame introduces an additional acceleration terms in the momentum equation.

$$\frac{\partial\rho}{\partial t}+\nabla.\rho\overrightarrow{v_r}=0 \tag{10}$$

$$\frac{\partial}{\partial t}(\rho\vec{v})+\nabla.(\rho\vec{v}_r\vec{v})+\rho(\vec{\omega}*\vec{v})=-\nabla p+\nabla\bar{\bar{\tau}}_r \tag{11}$$

The Coriolis and the centripetal accelerations are included in the momentum equation with the term $(\vec{\omega}*\vec{r})$.

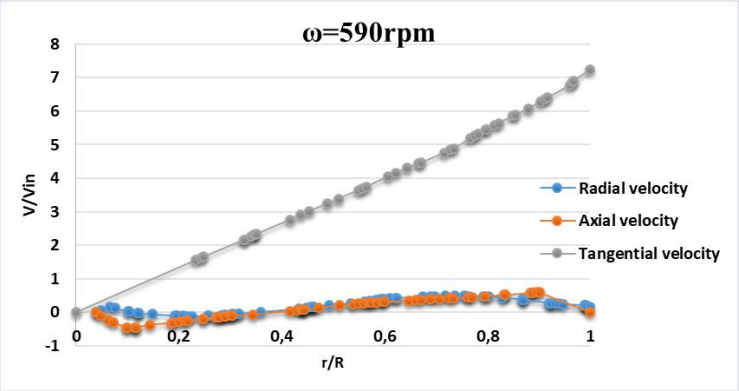

Fig. 5. Comparison of the dimensional tangential, axial and radial velocity components in the ACE rotor at z=30mm and ω=590rpm.

4. COMPUTATIONAL RESULTS

The simulated results of ACE rotor were used for validating the velocity predicted results with the experimental ones available in the literature and provided by Xu *et al.* (Yan, Jian-gang, Shuang-liang, & Zhi-shan, 2015).

4.1 CFD Model Validation

Figure 5 shows a comparison between tangential, axial, and radial velocity components across a cross section at a height of z=30 mm. In fact, according to this figure, it was clear that the magnitude of radial and axial velocities were much lower than the tangential velocity. The tangential velocity is the most dominant component in the extractors because it leads to large centrifugal action forces, which is responsible for the swirling motion of the fluid and for the separation phenomenon of the two phases in the considered extractors (Guizani, Mokni, Mhiri, & Bournot, 2014). That is why we focused on this component of the velocity in the validation study.

Indeed, we employed the standard different turbulence models to carry out the three-dimensional CFD simulations in the rotor region of the annular centrifugal extractor with the multiple reference frame (MRF). In addition, simulations were performed using the Re-normalized group (RNG) k–ε, the Reynolds stress, and the SST k–ω models of turbulence.

Figure 6 shows the comparison between the tangential velocity profiles for the tested turbulent models.

Results showed that the tangential velocity component could be predicted with the SST k- ω, the RNG models. It can be seen from Fig. 6 that the predicted results of these two models agree with the standard k- ε model. Based on these positive results, the validated k- ε model was used for investigating the effects of the shape of the separating blades in the flow field and performances of the rotor of the ACE.

Results showed that our numerical results for the tangential velocity component for rotor velocity 590 and 890 rpm are in good agreement compared to those experimentals made by Xu *et al.* However, for the rotor velocity of 1190 rpm, a slight deviation was denoted for the tangential velocity values near the middle of the rotor. This could be explained first by the more or less important errors slip in the experimental aspect. Furthermore, these differences between the values are because the geometrical dimensions of the integrated internals and the weirs were not given. Thus, we have estimated the dimensions of the rotor interior.

Figure 7 shows the comparison between the predicted and experimental path lines in the horizontal section z=5mm which is located between the rotor inlet and the diverter disc. It can be observed from Fig. 7 that the predicted streamlines of the fluid inside the rotational rotor is highly turbulent swirling flow and this latter spins in a clockwise direction that increases in a radial direction. The comparison of the CFD simulations with the experimental results shows a good agreement. So from these preceding results, it was concluded that the present CFD methodology could be valid for further simulations.

4.2 Comparison Investigation

In this part of our work, the flow field in the separating zone of ACE and the behavior of the dispersed phase (air) into the rotor are treated in order to compare the straight blades and the curved blades performances.

Indeed, we started the study by simulating the flow field when using straight separating blades in the rotor region of ACE. The studied domain is simulated for the multiphase flows and for a constant impeller rotational speed (N = 3000 rpm). In the water/air flows, as in the studied ACE rotor, we noticed the formation of the air core in the central region. That is why, it is essential to examine the two fluids in terms of the volume fraction of each phase in the whole studied area. Figure 8 shows the contours of the volume fraction on the yz plane for the two configurations of the ACE.

Moreover, the examination of the predicted and the experimental velocity vectors that are previously plotted in Figure 7 showed that the flow structures formed inside the ACE rotor are influenced by the vertical vanes. That is why we proposed to modify

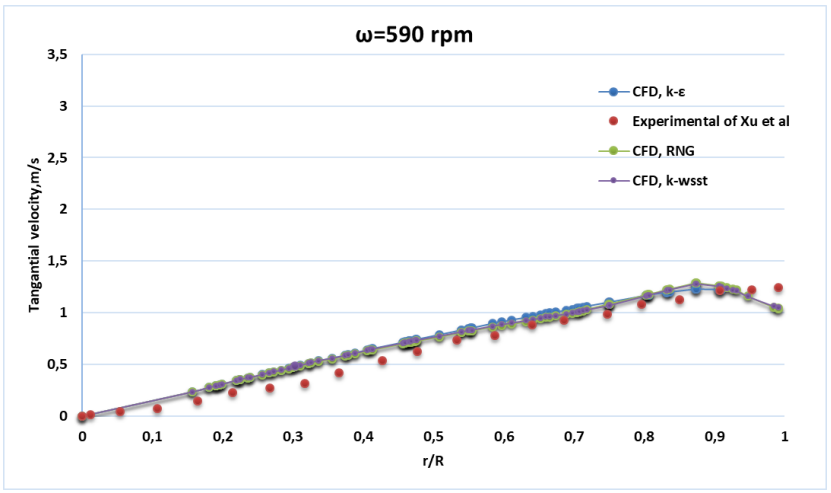

(a)

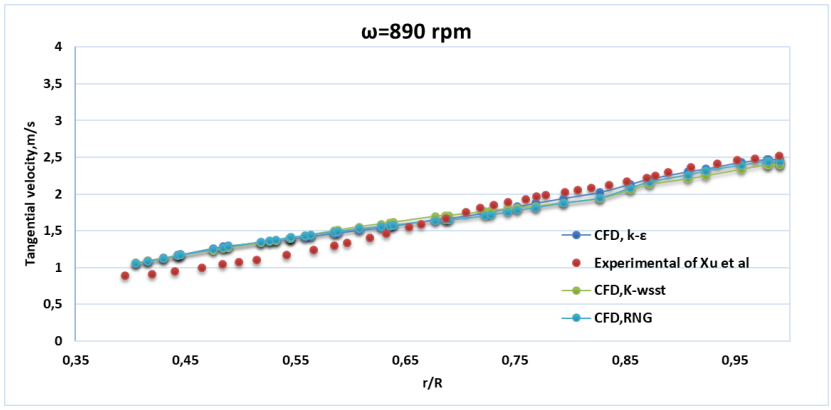

(b)

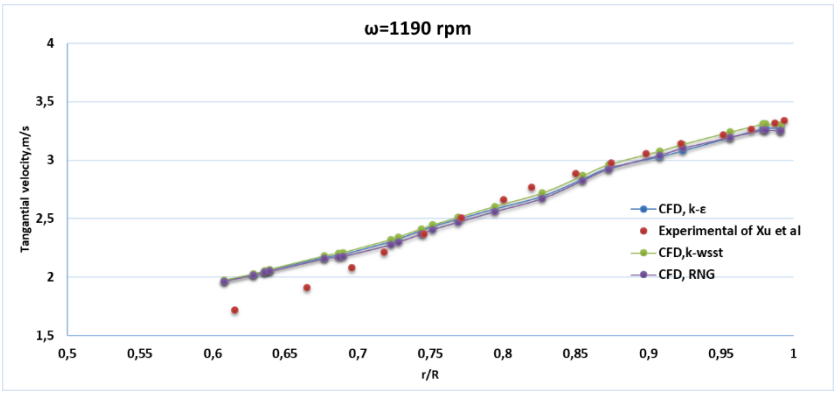

(c)

Fig. 6. Comparison between Radial profiles of tangential velocity for different turbulence models at z=30mm for rotor speeds (a)590rpm, (b) 890rpm and (c) 1190 rpm.

the curvature of the blades in order to enhance separation phenomenon by improving the velocity distribution in the ACE rotor.

4.2.1 Pressure profiles and Air Core

The pressure distributions inside the two different geometries of the ACE rotors and for different rotational speeds were investigated and CFD results are reported in Fig. 9 in order to understand the impact of the shape of the separating blades studied in the pressure field.

Figure 9 shows the contours of the static pressure on the **yz** plane for the two configurations of the ACE. According to this figure, a significant difference in the pressure distribution appeared in the central part of the rotating rotor with straight blades and with curved blades. The comparison of the results showed that the modification of the separation blades visibly affects the internal structure of the flow in the ACE rotor. This difference is clear especially in the central zone of the rotor where there is a strong depression for the rotor configuration with straight fins.

Figure 10 shows the radial profiles of the static pressure within the two-studied ACE rotors. From this figure, we noted that for the two rotor speeds

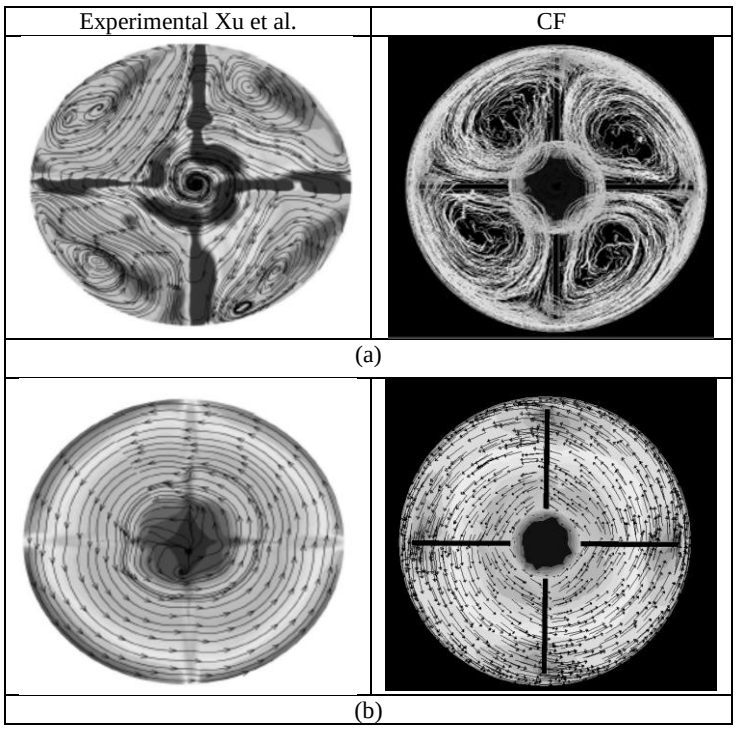

Fig. 7. Comparison between PIV experimental of (Yan, Jian-gang, Shuang-liang, & Zhi-shan, 2015) **and CFD results of (a) The velocity vectors relative to the ground and (b) the velocity vectors relative to the rotor, at z=5mm.**

ω=890 rpm and ω=1190 rpm and for the two axial positions z=5mm and z=30mm, the values of the static pressure of the geometry with curved blades is greater than with straight blades. However for a high rotor speed ω=2500rpm and ω=3000 rpm we noted that the static pressure of the ACE with curved blades is reduced compared with the straight blades. Besides, it can be seen that in both rotor geometries, there was an air core formed in the center of the rotor zone. The pressure of the air core in the separating zone of the ACE was lower than atmospheric pressure because of the pumping effect of the light phase outlets.

According to Figs. 9 and 10, it is clear that the effect of the geometry of the separating blades in the flow field is more prominent in the central area inside the rotary ACE.

4.2.2 Effects of the Shape of Separating Blades in the Pressure Drop:

The pressure drop across the rotor of the ACE was an important characteristic to the performance measurement since it is directly related to the operating costs.

The pressure drop over the rotor ACE with straight blades and with curved blades were investigated and CFD results are reported in Fig. 11. The pressure drop is obtained by integrating the pressure on the inlet and the exit faces. The rotor with curved blades operates at lower pressure drop than with straight blades when the rotational speed is greater than 2200 rpm and when ω is less than 2200 rpm, we noted that the ACE rotor with straight blades works at lower pressure.

Thus, pressure drop reduction due to ACE rotor with curved blades design reduces considerably power requirements. However, this criterion is insufficient to judge a performance of classification. It is necessary to compare also other detailed hydrodynamic information, such as the liquid hold-up volume and the interface radius, which are very important for successful design and operation of ACEs.

The Fluent code with the VOF multiphase model, predict very well the liquid holdup volume and the interface radius in the separation region of the ACE (Wardle K. E., Allen, Anderson, & Swaney, 2008) That we will try to prove in this study.

4.2.3 Effects of the Shape of Separating Blades in the Liquid Hold-Up Volume

Figure.12 shows the effects of the shape of the internals in the liquid hold-up of the ACE rotor.

The liquid hold-up volume of the rotor of the ACE includes the volumes of both the weir section and the separating zone. It is an important parameter that affects the fluid behavior, the inter-facial area and the overall extraction efficiency of the ACE.

The liquid hold-up volume of the rotor was obtained using the CFD simulation. The effects of the rotor speed on the liquid hold-up volume of the rotor are shown in Fig.12.

The liquid hold-up volume decrease initially with the increase of rotational speed, and then remains constant regardless of the shape of blades. Besides, we noted in Fig. 12 that the liquid hold-up volume of the rotor with curved blades was markedly lower than the rotor with curved blades**.**

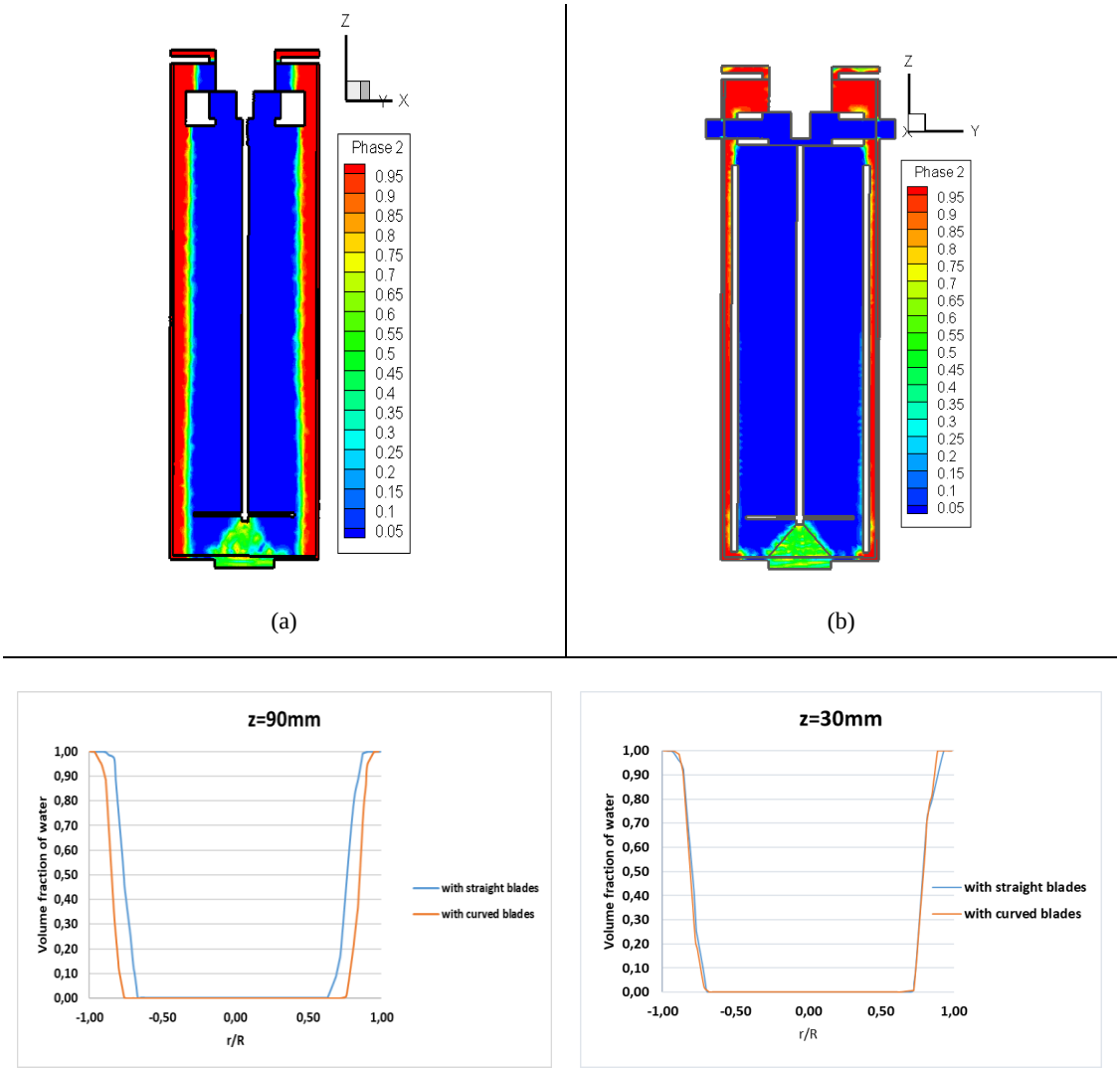

Fig. 8. Contours of the volume fraction of water in the permanent regime within the two studied rotor ACE, (a) rotor with straight blades, (b) rotor with curved blades, (c) Air/water interfaces for different heights z=90mm and z=30mm.

4.2.4 Effects of the Shape of Separating Blades in the Interface Radius:

Figure 13 shows the effects of the geometry of separating blades in the radius interface of the ACE rotor.

The light (air)-heavy phase (water) interface is formed as a vertical cylindrical surface. The effect of rotor speed (ω) on the interface radius is shown in Fig. 13. The values of r_i increases initially with the increase of (ω) and demure constant. We noted also, that the values of r_i for the rotor with curved blades is greater than the geometry with straight vanes in the range of ω = [1000-2200].

5. CONCLUSION

This study has presented the results of CFD calculations of the flow in the settling region of an annular centrifugal contactor.

The tangential velocity at various rotation speeds were compared with experimental results. A good agreement between the CFD predictions and the experimental measurements was obtained. The results proved that the k-ε turbulence model could describe accurately the flow pattern in the separation zone of the extractor in terms of streamlines, static pressure distribution and velocity profiles.

The separation phenomenon in an ACE rotor has been investigated by CFD analysis. Standard k-ε and volume of fluid models have been used to model the turbulence nature and the multiphase flow of the ACE rotor.

The CFD results for a range of rotor speeds were performed to characterize the flow of water in the settling region of the ACE using two different separating blades geometries.

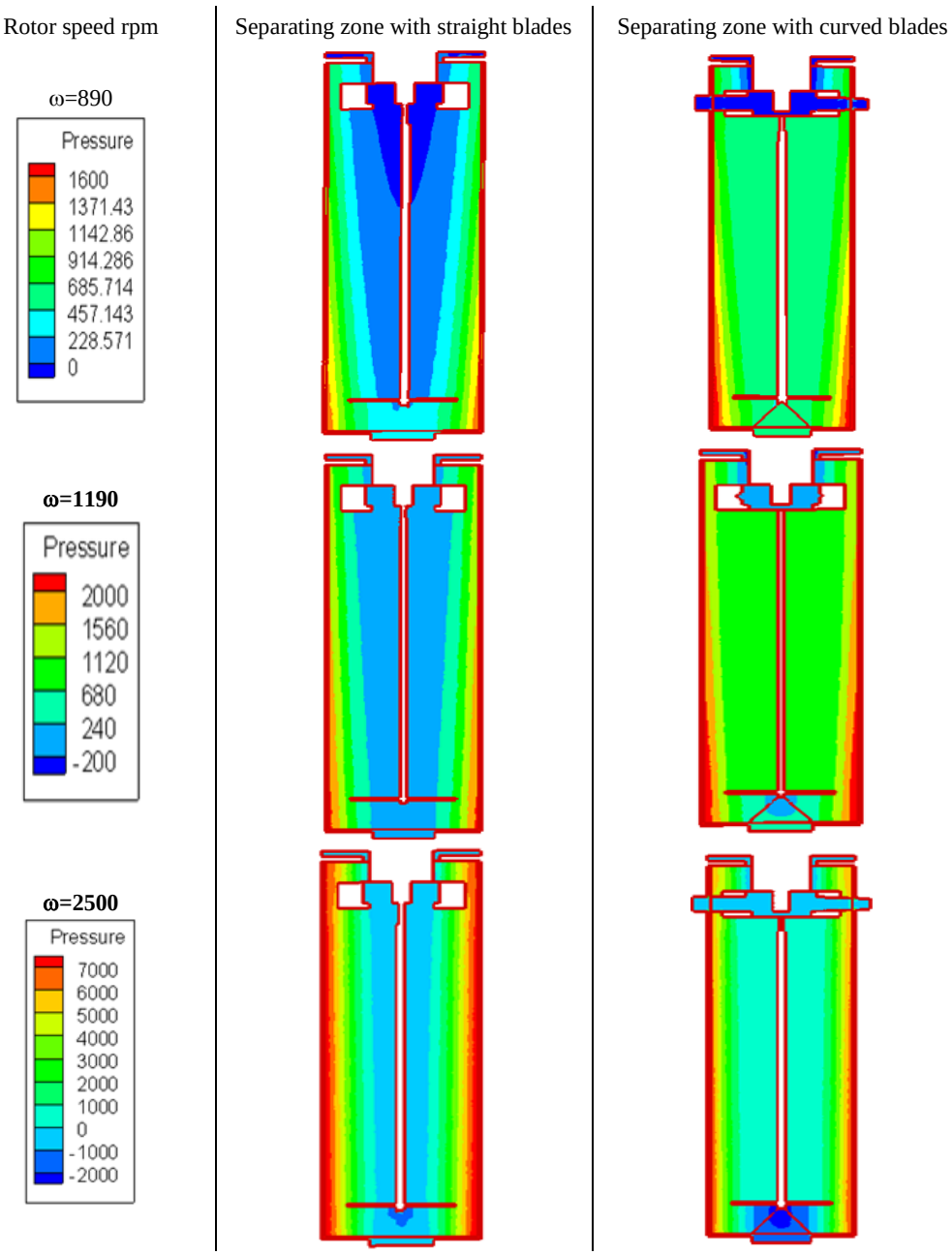

Fig. 9. Effects of the shape of separating blades and the rotor velocity on the pressure field inside the ACE rotor.

It was found that the flow inside the rotor is turbulent forced vortex flow for the two types of the ACE rotor. Besides, we noticed that the static pressure for both geometries is highest near the wall and decrease gradually with respect to the radial distance from the wall to the center, which provides the separation of the heavy phase fluid to be separated from the light phase fluid in order to be derived to the appropriate outlet. In addition, we noticed that the geometry of the separating blades in the flow field is more prominent in the central area inside the rotary ACE. However, the central region in the rotor is highly influenced with the geometry of internals, which prevents the increase of the static pressure in the axis of rotation and the central vortex.

Besides, the predicted pressure drop proved that the geometry of the ACE rotor with curved blades leads to a lower values of pressure drop which is related to the power consumption of energy for rotor speeds superior to ω=2200 rpm. Thus, the pressure drop to ACE rotor with curved blades design reduces considerably power requirements geometry of the vertical separating blades.

In addition, it was found that curved blades has a significant impact on the liquid hold-up, in the interface radius and on the general flow in the separating zone.

It is to be noted that the CFD tools provide details on the entire flow field inside the ACE rotor not possible

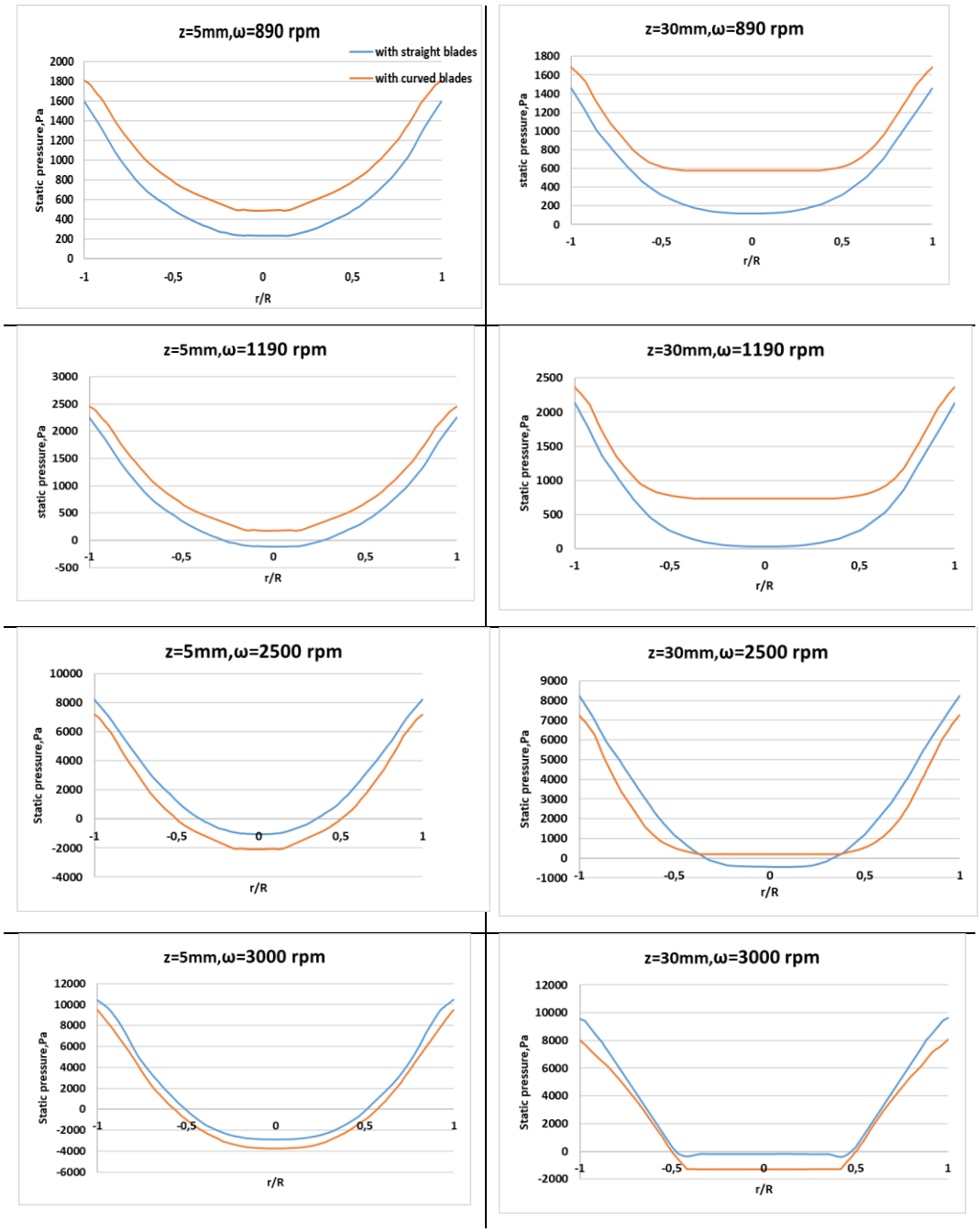

Fig. 10. Radial profiles of static pressure within the two studied rotor ACE at two axial positions z=5mm and z=30mm for rotor speeds ω=890, 1190, 2500 and 3000rpm.

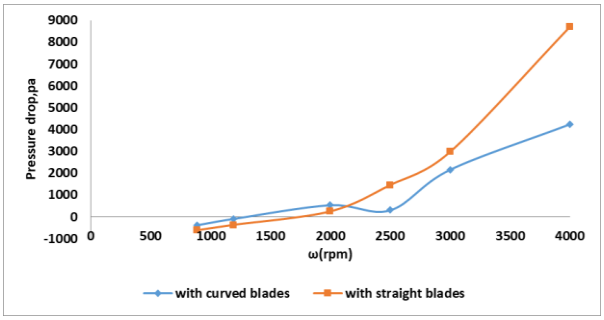

Fig. 11. Effects of the shape of separating blades in the pressure drop of the ACE rotor.

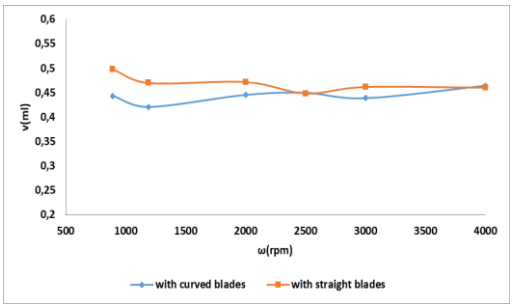

Fig. 12.Effects of the shape of separating blades in the liquid hold-up of the ACE rotor.

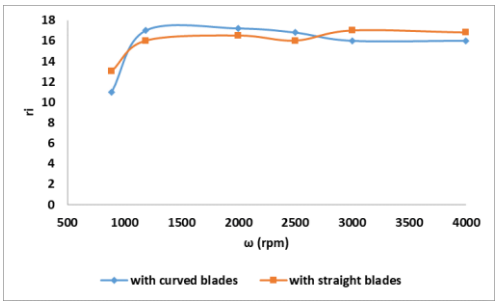

Fig. 13. Effects of the shape of separating blades in the radius interface of the ACE rotor.

by experimentation over a wide range of rotational speeds. These qualitative predictions can be exploited in order to enhance the performances of this equipment.

We must note that the design of the vertical vanes is very sensitive and complex. This study provides a starting point for simulating the high turbulent flow inside the moving ACE rotor in order to gain the confidence to go further and model increasingly more complex cases.

So we wish to add more complexities in a further stepwise manner and we will try to study the effect of the geometry and the form of the diverter disk in the separation region.

REFERENCES

Achouri, R., I. Mokni, H. Mhiri and P. Bournot (2012). A 3D CFD simulation of a self inducing Pitched Blade Turbine Downflow. *Energy conversion and management 64*, 633-641.

Arafat, H., M. Hash, A. S. Hebben and R. Leonards (2001). Characterization and Recovery of Solvent Entrained During the Use of Centrifugal Contactors. *Argonne National Laboratory, III*(ANL-02), 8.

Bernstein, G., D. Grosvenor, J. Lenc and N. Levitz (1973). A high capacity annular centrifugal contactor. *Nuclear Technology* (20), 200–202.

Boelo, S., N. Kraai, G., G. M. Winkelman, J., and J. Heeres, H. (2012). Hydrodynamic features of centrifugal contactor separators: Experimental studies on liquid hold-up, residence time distribution, phase behavior and drop size distributions. *Chemical Engineering and Processing: Process Intensification, 55*, 8-19.

Chouari, Y., W. Kriaa, H. Mhiri and P. Bournot (2017). CFD investigation on mixing in a rapidly mixed tubular flame burner. *Meccanica* 52(15), 3615-3627.

Deshmukh, S. S., S. Vedantam and J. B. Joshi (2008). Flow Visualization and Three-Dimensional CFD Simulation of the Annular. *Industrial & Engineering Chemistry Research 47*, 3677–3686.

Deshmukh, S. S., S. Vedantam, J. B. Joshi and S. B. Koganti (2007). Computational flow modeling and visualization in the annular region of annular centrifugal extractor. *Industrial & Engineering Chemistry Research 46*, 8343–8355.

FLUENT 6.3, D. (2001). *User's Guide Fluent.* Récupéré sur sharcnet: https://www.sharcnet.ca/Software/Fluent6/index.htm

Gandhi, N. N., S. B. Sawant and J. B. Joshi (1995). Specificity of a lipase in ester synthesis: effect of alcohol. *Biotechnology Progress* 11(3), 282–287.

Guizani, R., I. Mokni, H. Mhiri and P. Bournot (2014). CFD modeling and analysis of the fish-hook effect on the rotor separator's efficiency. *Powder Technology* 264, 149-157.

Imamura, T., K. Saito and S. A. Ishikura (1993). New approach to continuous emulsion polymerization. *Polymer International 30*(2), 203–206.

Jing, X., P. Ning, H. Cao, J. Wang and Z. Sun (2018). A review of application of annular centrifugal contactors in aspects of mass transfer and operational security. *Hydrometallurgy*.

Kataoka, K., N. Ohmura, M. Kouzu, Y. Simamura and M. Okubo (1995). Emulsion polymerization of styrene in a continuous Taylor vortex flow reactor. *Chemical Engineering Science* 50(9), 1409–1416.

Khaldi, N., H. Mhiri and P. Bournot (2014). Prediction of pollutant dispersion in turbulent two-phase flows. *Environmental Fluid Mechanics 14*(3), 647-662.

Leonard, P. R., A. Ziegler and G. Bernstein (1980). Flow over Circular Weirs in a Centrifugal Field. *The Canadian Journal of Chemical Engineering* 58,531.

Leonard, R., G. Bernstein, R. Pelto and A. Ziegler (1981). Liquid-Liquid Dispersion in Turbulent Couette Flow. *AIChE J.* 27,495.

Mokni, I., H. Dhaouadi, P. Bournot and H. Mhiri (2015). Numerical investigation of the effect of the cylindrical height on separation performances of uniflow hydrocyclone.

Chemical Engineering Science(122), 500-513.

Ogihara, N., G. Matsuda, T.Yanagawa, N. Ogata, K. Fujita and M. Nomura (1995). Continuous synthesis of monodispersed silica particles using Couette-Taylor vortex flow. *Journal of the Ceramic Society of Japan* 103, 151–154.

Padial-Collins, N. T., D. Z. Zhang, Q. Zou and X. Ma (2006). Centrifugal contactors: Separation of an aqueous and an organic stream in the rotor zone. *Separation Science and Technology 41*, 1001–1023.

Patra, J., N. K. Pandey, U. K. Muduli, R. Natarajan and J. B. Joshi (2013). Hydrodynamic study of flow in the rotor region of annular centrifugal contactors using CFD simulation. *Chemical Engineering Communications* 200(4), 471-493.

Sathe, M. J., S. S. Deshmukh, J. B. Joshi and S. B. Koganti (2010). Computational fluid dynamics simulation and experimental investigation: study of two-phase liquid-liquid flow in a vertical Taylor-Couette contactor. *Industrial & Engineering Chemistry Research* 49(1), 14–28.

Shaowei, L., D. Wuhua, C. Jing and W. Jianchen (2012). CFD Simulation of Gas-Liquid-Liquid Three-Phase Flow in an Annular Centrifugal Contactor. *Industrial & Engineering Chemistry Research* 51, 11245-11253.

Wardle, K. E., T. R. Allen and R. Swaney (2009). CFD simulation of the separation zone of an annular centrifugal contactor. *Separation Science and Technology 44*(3), 517-542.

Wardle, K. E., T. R. Allen, M. H. Anderson and R. E. Swaney (2008). Free surface flow in the mixing zone of an annular centrifugal contactor. *AIChE Journal* 54(1), 74-85.

Wardle, K., T. Allen, M. Anderson and R. Swaney (2009). Analysis of the effect of mixing vane geometry on the flow in an annular centrifugal contactor. *AIChE J.*, In press.

Yan, X., W. Jian-gang, Z. Shuang-liang and B. Zhi-shan (2015). PIV experimental study on the flow field in the rotor zone of an annular centrifugal contactor. *Chemical engineering research and design 94*, 691–701.

Zhou, J., W. Duan, X. Zhou and C. Zhang (2007). Application of annular centrifugal contactors in the extraction flowsheet for producing high purity yttrium. *Hydrometallurgy* 85(2-4), 154-162.